Imaging Algorithm of Missile-borne SAR in Diving and Squint Mode

Zhen Wang, Xiaodong He and Bin Tang
School of Electronic Engineering, University of Electronic Science and Technology of China, Sichuan, China
jeannewang1990@gmail.com

Abstract - In this paper, we propose an imaging algorithm of missile-borne SAR in diving and squint mode. The diving acceleration, vertical speed, and squint angle caused a large range cell migration (RCM). The algorithm divides the RCM correction (RCMC) into two steps. Firstly, correcting the main part of range walk in time domain. Secondly, correcting the remaining RCMC in range frequency-azimuth Doppler frequency domain, using an analytical form of the signal 2-D spectrum derived by the method of series reversion. Theoretical analysis and simulation results illustrate its validity, and satisfy the imaging quality of missile-borne SAR in high squint model.

Index Terms - Missile-borne SAR, diving and squint mode, RCMC, series reversion.

I. Introduction

Compared with general airborne or space-borne SAR, missile-borne SAR has significantly different characteristics. In order to attack the target, missile-borne SAR cannot do the uniform line motion, and also it has a certain acceleration and vertical velocity in the diving flight. Moreover, it usually works in a squint mode in order to acquire a period of turning time. Therefore, the general SAR imaging algorithms are no longer suitable for missile-borne SAR [1-2].

In [3], the 2-D spectrum of target echo was derived by the method of series reversion, and the RCMC, range and azimuth compression were accomplished in the 2-D frequency domain. But the algorithm was only suitable for the center single point target imaging of the scene in side-looking mode. An imaging algorithm for missile-borne SAR based on azimuth nonlinear chirp scaling (NLCS) was proposed in [4]. After finished RCMC and range compression in the 2-D frequency domain by the method of series reversion, azimuth variation of Doppler FM rates for echo signal were compensated with the operation of azimuth NLCS, which could improve focusing depth and effect. However, the computation is too heavy, and it also only worked in side-looking mode. In [5], the spectral overlapping phenomenon in distance was solved by introducing a new CS factor, and the influence caused by velocity and acceleration of the missile were compensated. A deramp method was introduced to cope with the Doppler spectral overlapping phenomenon in azimuth, but this algorithm was too complex to realize.

According to the characteristics of the missile-borne SAR platform motion, a space geometry relationship of the diving and squint movement is established in this paper. Then the instantaneous range between radar and target is calculated, and the point target echo signal model is derived. The Doppler frequency center is corrected in range frequency-azimuth time domain [6]. The 2-D spectrum of the point target echo signal is deduced using the method of series reversion. After finishing the pulse compression processing, a focused point target image is got. At last, a missile-borne SAR simulation is used to illustrate its validity of the algorithm.

II. Geometric Model and Instantaneous Range

The imaging geometry of missile-borne SAR is shown in Fig. 1. A missile is assumed to be flying along the trajectory of ABC with a constant acceleration in a two-dimensional plane, which is locally vertical to the surface of the Earth and the projection of trajectory on the ground is X axis. The range time is given by t_r, and the azimuth time t_a is chosen to be zero at the composite beam center crossing time (mid exposure time) of the reference target. V is the velocity of the missile, and the horizontal and vertical velocity are V_x and V_z, accompanying with the constant acceleration a_x and a_z. While the velocity and acceleration are all zero. H is the height of the missile at $t_a = 0$. The instantaneous range from SAR to an arbitrary reference point target $P(x_0, y_0, 0)$ is R_0, and The shortest range R_c has a relationship with R_0 and squint angle θ, which is $R_c = R_0 \cos\theta$.

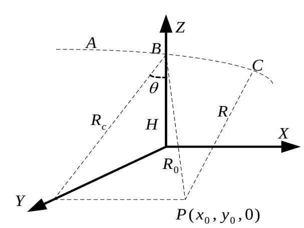

Fig. 1 The diving and squint missile-borne SAR geometry.

The instantaneous range from SAR to a point target at azimuth time t_a can be expressed as

$$R(t_a, R_0) = \sqrt{\begin{array}{l} R_0^2 + (V_x t_a + \frac{1}{2} a_x t_a^2 - x_0)^2 \\ -2R_c (V_x t_a + \frac{1}{2} a_x t_a^2 - x_0) \sin\theta \\ +(V_z t_a + \frac{1}{2} a_z t_a^2)^2 + 2H(V_z t_a + \frac{1}{2} a_z t_a^2) \end{array}} \tag{1}$$

The first 5th order Taylor expansion [7] of (1) can be expressed as

$$R(t_a;R_0) \approx k_{00} + k_{10}t_a + k_{20}t_a^2 + k_{30}t_a^3 + k_{40}t_a^4 + 0(t_a^5) \quad (2)$$

Letting $w_1 = -V_x x_0 + HV_z - R_c V_x \sin\theta$, $w_2 = V_x^2 + V_z^2 - a_x x_0 + Ha_z - R_c a_x \sin\theta$, $w_3 = V_x a_x + V_z a_z$, $w_4 = a_x^2 + a_z^2$, $R_x = \sqrt{R_0^2 + x_0^2 + 2R_c x_0 \sin\theta}$, $a_1 = -V_x x_0 / R_x$. Then, the coefficients in (2) can be expressed as

$$\begin{cases} k_{00} = R_x, k_{10} = \frac{w_1}{R_x} = a_1 + \frac{HV_z}{R_x} + \frac{-R_c V_x \sin\theta}{R_x}, \\ k_{20} = \frac{w_2}{2R_x} - \frac{w_1^2}{2R_x^3}, k_{30} = \frac{w_3}{2R_x} - \frac{w_1 w_2}{2R_x^3} + \frac{w_1^3}{2R_x^5}, \\ k_{40} = \frac{w_4}{8R_x} - \frac{w_2^2 + 4w_1 w_3}{8R_x^3} + \frac{3w_1^2 w_2}{4R_x^5} - \frac{5w_1^4}{8R_x^7} \end{cases} \quad (3)$$

III. Analysis of Signal and Imaging Algorithm

A. Derivation of the Signal Spectrum

Assuming the transmitted LFM signal is

$$s_t(t_r, t_a; R_0) = a_r(t_r)\exp(j2\pi f_c t_r + j\pi\gamma t_r^2) \quad (4)$$

where f_c is the carrier frequency, γ is the range chirp rate, $a_r(\cdot)$ and is $a_a(\cdot)$ are the range and azimuth envelopes.

The echo received from a reference point target experiences a delay that is proportional to the two-way slant range $2R(t_a;R_0)$. After down-converted to baseband, it can be expressed with range time t_r and azimuth time t_a as

$$\begin{aligned} s(t_r, t_a; R_0) &= s_t(t_r - 2R(t_a;R_0)/c, t_a; R_0) \\ &= a_r(t_r - 2R(t_a;R_0)/c)a_a(t_a) \\ &\exp[-j\frac{4\pi}{\lambda}R(t_a;R_0)]\exp[j\pi\gamma(t_r - 2R(t_a;R_0)/c)^2] \end{aligned} \quad (5)$$

where λ is the radar wavelength, c is the speed of light.

Using Principal of Stationary Phase (POSP) and Fresnel Integral [8], the range FT of (5) can be expressed as

$$\begin{aligned} S(f_r, t_a; R_0) &= \int s(t_r, t_a; R_0)\exp(-j2\pi f_r t_r)dt_r \\ &= a_r(f_r)a_a(t_a)\exp(-j\frac{\pi f_r^2}{\gamma}) \\ &\exp[-j4\pi\frac{f_r + f_c}{c}R(t_a;R_0)] \end{aligned} \quad (6)$$

where f_r is the range frequency. Then the Doppler center frequency of range can be given by

$$f_{dc} = -\frac{2}{\lambda}\frac{dR(t_a;R_0)}{dt_a}\Big|_{t_a=0} = -\frac{2}{\lambda}(a_1 + \frac{HV_z}{R_x} - \frac{R_c V_x \sin\theta}{R_x}) \quad (7)$$

where $\frac{HV_z}{R_x} - \frac{R_c V_x \sin\theta}{R_x}$ is the Doppler frequency offset which is caused by the vertical velocity and squint angle. It should be corrected through the correction function as follows.

$$H_1 = \exp[-j4\pi\frac{f_r + f_c}{c}(-\frac{HV_z}{R_x} + \frac{R_c V_x \sin\theta}{R_x})t_a] \quad (8)$$

The result of Doppler frequency offset correction can be written as

$$\begin{aligned} &S_1(f_r, t_a; R_0) = a_r(f_r)a_a(t_a)\exp(-j\frac{\pi f_r^2}{\gamma}) \\ &\exp[-j4\pi\frac{f_r + f_c}{c}(R_x + a_1 t_a + k_{20}t_a^2 + k_{30}t_a^3 + k_{40}t_a^4)] \end{aligned} \quad (9)$$

Letting

$$R_1(t_a;R_0) = R_{cen} + k_2 t_a^2 + k_3 t_a^3 + k_4 t_a^4 \quad (10)$$

where, $R_{cen} = 2R_x$, $k_1 = 2a_1$, $k_2 = 2k_{20}$, $k_3 = 2k_{30}$, $k_4 = 2k_{40}$.

After Doppler frequency offsetting, it can be expressed as

$$\begin{aligned} s_1(t_r, t_a; R_0) &= a_r(t_r - \frac{R_1(t_a;R_0)}{c} - \frac{k_1 t_a}{c})a_a(t_a) \\ &\exp[j\pi\gamma(t_r - \frac{R_1(t_a;R_0)}{c} - \frac{k_1 t_a}{c})^2] \\ &\exp[-j\frac{2\pi}{\lambda}R_1(t_a;R_0)]\exp(-j2\pi\frac{f_c k_1 t_a}{c}) \end{aligned} \quad (11)$$

Letting

$$\begin{aligned} s_A(t_r, t_a; R_0) &= a_r(t_r - \frac{2R_1(t_a;R_0)}{c})a_a(t_a) \\ &\exp[j\pi\gamma(t_r - \frac{2R_1(t_a;R_0)}{c})^2]\exp[-j\frac{4\pi}{\lambda}R_1(t_a;R_0)] \end{aligned} \quad (12)$$

Equation (11) can be expressed as follows.

$$s_1(t_r, t_a; R_0) = s_A(t_r - \frac{k_1 t_a}{c}, t_a; R_0)\exp(-j2\pi\frac{f_c k_1 t_a}{c}) \quad (13)$$

Using the methods of POSP and Fresnel Integral, we get the range FT of (13)

$$\begin{aligned} S_A(f_r, t_a; R_0) &= a_r(f_r)a_a(t_a)\exp(-j\frac{\pi f_r^2}{\gamma}) \\ &\exp[-j2\pi\frac{(f_r + f_c)}{c}R_1(t_a;R_0)] \end{aligned} \quad (14)$$

According to the methods of POSP and series reversion [9], we get

$$-\frac{c}{(f_c + f_r)}f_a = 2k_2 t_a + 3k_3 t_a^2 + 4k_4 t_a^3 \quad (15)$$

Using the method of series reversion [9] with (15), we obtain the stationary phase point

$$t_a^* = A_1(-\frac{f_a c}{f_c + f_r}) + A_2(-\frac{f_a c}{f_c + f_r})^2 + A_3(-\frac{f_a c}{f_c + f_r})^3 \quad (16)$$

where $A_1 = \frac{1}{2k_2}$, $A_2 = -\frac{3k_3}{8k_2^3}$, $A_3 = \frac{9k_3^2 - 4k_2 k_4}{16k_2^5}$.

Therefore, the azimuth FT of (14) is

$$\begin{aligned} S_A(f_r, f_a; R_0) &= a_r(f_r)a_a(f_a)\exp(-j\frac{\pi f_r^2}{\gamma}) \\ &\exp\{-j2\pi[\frac{f_c + f_r}{c}R_1(t_a^*;R_0) + f_a t_a^*]\} \end{aligned} \quad (17)$$

The phase of the second exponential can be expanded as

$$
\begin{aligned}
&\frac{f_c+f_r}{c}R_1(t_a^*;R_0)+f_a t_a^*=\frac{f_c+f_r}{c}R_{cen}\\
&+\frac{A_1^2k_2c-A_1c}{f_c+f_r}f_a^2\\
&+\frac{-(-A_2+2A_1A_2k_2+A_1^3k_3)c^2}{(f_c+f_r)^2}f_a^3\\
&+\frac{(-A_3+2A_1A_3k_2+A_2^2k_2+A_1^4k_4+3A_1^2A_2k_3)c^3}{(f_c+f_r)^3}f_a^4\\
&+\frac{-(2A_2A_3k_2+3A_1^2A_3k_3+3A_1A_2^2k_3+4A_1^3A_2k_4)c^4}{(f_c+f_r)^4}f_a^5+\cdots
\end{aligned}
\tag{18}
$$

According to the properties of FT, the 2-D FT of $s_1(t_r,t_a;R_0)$ is

$$
S_1(f_r,f_a;R_0)=S_A(f_r,f_a+(f_c+f_r)\frac{k_1}{c};R_0) \tag{19}
$$

The effect of the high order terms of f_a for phase is far less than $\pi/4$, so we keep the terms of (18) up to the first 4th order of f_a. Then (19) can be written as

$$
S_1(f_r,f_a;R_0)=a_r(f_r)a_a(f_a)\exp[j\varphi(f_r,f_a)] \tag{20}
$$

where, the phase function $\varphi(f_r,f_a)$ can be expanded as

$$
\begin{aligned}
\varphi(f_r,f_a)=&-2\pi\frac{f_c+f_r}{c}R_{cen}-\frac{\pi f_r^2}{\gamma}\\
&+2\pi\frac{c}{4k_2(f_c+f_r)}[f_a+(f_c+f_r)\frac{k_1}{c}]^2\\
&+2\pi\frac{c^2k_3}{8k_2^3(f_c+f_r)^2}[f_a+(f_c+f_r)\frac{k_1}{c}]^3\\
&+2\pi\frac{c^3(9k_3^2-4k_2k_4)}{64k_2^5(f_c+f_r)^3}[f_a+(f_c+f_r)\frac{k_1}{c}]^4
\end{aligned}
\tag{21}
$$

And, the term $\frac{1}{f_c+f_r}$, and its expressions of square and cubic value can be also expanded as follows, respectively.

$$
\begin{cases}
\frac{1}{f_c+f_r}\approx\frac{1}{f_c}(1-\frac{f_r}{f_c}+\frac{f_r^2}{f_c^2}-\frac{f_r^3}{f_c^3})\\
\frac{1}{(f_c+f_r)^2}\approx\frac{1}{f_c^2}(1-2\frac{f_r}{f_c}+3\frac{f_r^2}{f_c^2}-4\frac{f_r^3}{f_c^3})\\
\frac{1}{(f_c+f_r)^3}\approx\frac{1}{f_c^3}(1-3\frac{f_r}{f_c}+6\frac{f_r^2}{f_c^2}-10\frac{f_r^3}{f_c^3})
\end{cases}
\tag{22}
$$

Then, (21) can be written as follows.

$$
\varphi(f_r,f_a)=\varphi_0(f_a)+\varphi_1(f_a)f_r+\varphi_2(f_a)f_r{}^2+\varphi_3(f_a)f_r{}^3 \tag{23}
$$

Each of these phase terms are list as follows.

$$
\begin{aligned}
\varphi_0(f_a)=&-\frac{2\pi f_cR_{cen}}{c}+\frac{\pi f_ck_1^2}{2ck_2}+\frac{\pi f_ck_1^3k_3}{4ck_2^3}+\frac{\pi f_c(9k_3^2-4k_2k_4)k_1^4}{32k_2^5c}\\
&+\frac{\pi k_1f_a}{k_2}+\frac{3\pi k_1^2k_3f_a}{4k_2^3}+\frac{\pi(9k_3^2-4k_2k_4)k_1^3f_a}{8k_2^5}\\
&+\frac{\pi cf_a^2}{2f_ck_2}+\frac{3\pi ck_1k_3f_a^2}{4k_2^3f_c}+\frac{\pi 3c(9k_3^2-4k_2k_4)k_1^2f_a^2}{16k_2^5f_c}\\
&+\frac{\pi c^2k_3f_a^3}{4f_c^2k_2^3}+\frac{\pi c^2(9k_3^2-4k_2k_4)k_1f_a^3}{8k_2^5f_c^2}\\
&+\frac{\pi c^2(9k_3^2-4k_2k_4)f_a^4}{32k_2^5f_c^3}
\end{aligned}
\tag{24}
$$

$$
\begin{aligned}
\varphi_1(f_a)=&-\frac{2\pi R_{cen}}{c}+\frac{\pi k_1^2}{2ck_2}+\frac{\pi k_1^3k_3}{4ck_2^3}+\frac{\pi(9k_3^2-4k_2k_4)k_1^4}{32k_2^5c}\\
&-\frac{\pi cf_a^2}{2k_2f_c^2}-\frac{3\pi ck_1k_3f_a^2}{4k_2^3f_c^2}-\frac{3\pi c(9k_3^2-4k_2k_4)k_1^2f_a^2}{16k_2^5f_c^2}\\
&-\frac{\pi c^2k_3f_a^3}{2k_2^3f_c^3}-\frac{\pi c^2(9k_3^2-4k_2k_4)k_1f_a^3}{4k_2^5f_c^3}\\
&-\frac{3\pi c^3(9k_3^2-4k_2k_4)f_a^4}{32k_2^5f_c^4}
\end{aligned}
\tag{25}
$$

$$
\begin{aligned}
\varphi_2(f_a)=&-\frac{\pi}{\gamma}\\
&+\frac{\pi cf_a^2}{2k_2f_c^3}+\frac{3\pi ck_1k_3f_a^2}{4k_2^3f_c^3}+\frac{3\pi c(9k_3^2-4k_2k_4)k_1^2f_a^2}{16k_2^5f_c^3}\\
&+\frac{3\pi c^2k_3f_a^3}{4k_2^3f_c^4}+\frac{3\pi c^2(9k_3^2-4k_2k_4)k_1f_a^3}{8k_2^5f_c^4}\\
&+\frac{3\pi c^3(9k_3^2-4k_2k_4)f_a^4}{16k_2^5f_c^5}
\end{aligned}
\tag{26}
$$

$$
\begin{aligned}
\varphi_3(f_a)=&-\frac{\pi cf_a^2}{2f_c^4k_2}-\frac{3\pi ck_3k_1f_a^2}{4f_c^4k_2^3}-\frac{3\pi c(9k_3^2-4k_2k_4)k_1^2f_a^2}{16f_c^4k_2^5}\\
&-\frac{\pi c^2(9k_3^2-4k_2k_4)k_1f_a^3}{2f_c^5k_2^5}-\frac{\pi c^2k_3f_a^3}{f_c^5k_2^3}\\
&-\frac{5\pi c^3(9k_3^2-4k_2k_4)f_a^4}{16f_c^6k_2^5}
\end{aligned}
\tag{27}
$$

In (23), $\varphi_0(f_a)$ is azimuth modulation term and has no relationship with f_r. $\varphi_1(f_a)$ is the linear item coefficient of f_r. $\varphi_2(f_a)$ is the range chirp rate, and $\varphi_3(f_a)$ is the changing rate of the range chirp rate.

B. *Imaging Algorithm*

The flow chart of the algorithm is shown in Fig. 2.

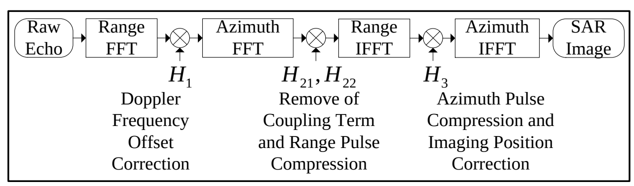

Fig. 2 The flow chart of the imaging algorithm

In (24), The linear item coefficient of f_a is $-2\pi(-\frac{k_1}{2k_2}-\frac{3k_1^2k_3}{8k_2^3}-\frac{(9k_3^2-4k_2k_4)k_1^3}{16k_2^5})$, which indicates the azimuth position of the target. In order to getting the correct azimuth position, we need to make imaging position correction during azimuth compression. The term $-2\pi R_{cen}/c$ in (25) indicates the range position of the target, and the remaining terms in (25) are RCM which are also being corrected.

The steps of the diving and squint missile-borne SAR are as follows.

Step1. Getting $S(f_r,t_a;R_0)$ through range FT of (5);

Step2. Correcting the Doppler frequency offset of $S(f_r,t_a;R_0)$ by multiplying H_1;

Step3. Getting 2-D spectrum $S_1(f_r, f_a; R_0)$ through azimuth FT of $S_1(f_r, t_a; R_0)$;

Step4. Removing the coupling term of $S_1(f_r, f_a; R_0)$ by

$$H_{21} = \exp[-j(\varphi_1(f_a) + R_{cen} 2\pi / c) f_r] \exp[-j\varphi_3(f_a) f_r^3] \tag{28}$$

And getting the result of range pulse compression by

$$H_{22} = \exp[-j\varphi_2(f_a) f_r^2] \tag{29}$$

Then, we get $S_1(t_r, f_a; R_0)$ through range IFT.

Step5. Getting the result of azimuth pulse compression by

$$H_3 = \exp[-j(\varphi_0(f_a) - \pi k_1 f_a / k_2)] \tag{30}$$

After azimuth IFT, we get the focusing SAR image.

When calculating a_1, R_c, w_1, w_2, w_3 and w_4, the values of x_0 and y_0 can be replaced by the coordinates X_c and Y_c of the imaging center.

IV. Simulation Results

We present some missile-borne SAR images generated by the proposed method in this paper. All the simulation results are shown on slant range plane. The designed scene consist some point targets, and the system parameters are list in TABLE 1.

TABLE 1 The simulation parameters

Parameters	Numerical Value
Carrier frequency f_c	35GHz
Pulse duration T_r	5μs
Bandwidth B_r	75MHz
Imaging center coordinate $(X_c, Y_c, 0)$	(0,4000m,0)
Initial flight altitude H	10000m
Initial Velocity (V_x, V_y, V_z)	(2000m/s,0,-100m/s)
Acceleration (a_x, a_y, a_z)	(-50m/s^2,0,-9.8m/s^2)
Antenna Azimuth length D	1m
Sampling frequency f_s	200MHz
PRF	20kHz
Squint angle	42°

Fig. 3 shows the results of pulse compression responses of point target. Fig. 3(a) shows the azimuth compression of point target, and Fig. 3(b) shows the azimuth compression of point target. Fig. 4 shows the contour plot of a point target. The quality parameters are list in TABLE 2. The simulation results illustrate focusing performance of the method proposed in this paper meets the requirements of missile-borne SAR in diving and squint mode. The algorithm uses only four Fourier transforms and four complex multiplications, without any interpolation operation, and the operation efficiency is greatly improved.

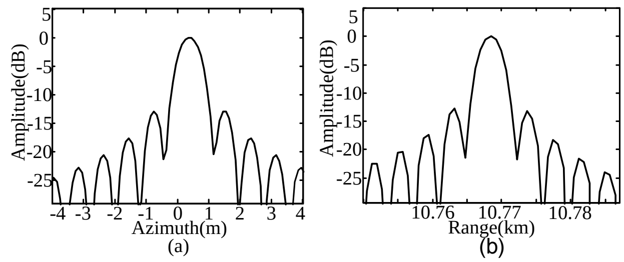

Fig. 3 The results of one point target. (a) Magnitude of Azimuth slices. (b) Magnitude of Range slices.

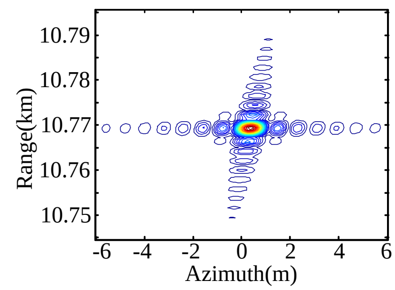

Fig. 4 Contour plot of the point target.

TABLE 2 Point target quality parameters

Parameters	Range direction	Azimuth direction
Resolution(m)	2	0.5
PSLR(dB)	-13.19	-12.93
ISLR(dB)	-10.01	-9.94

V. Conclusions

This paper presents an imaging algorithm for the diving and squint missile-borne SAR. The algorithm derives the 2-D frequency expression about echo signal of point target using the method of series reversion, and divides the RCM correction into main range walk correcting in time domain and remaining RCM correcting in range frequency-azimuth Doppler frequency domain. After the improvements about the current imaging algorithm of missile-borne squint SAR, we get a focused image. The point targets simulation results are presented to demonstrate its accuracy and validity of the proposed algorithm.

References

[1] Li Daojing, Zhang Linxi, Yu Bianzhang, "Research on active radar imaging seeker," *Modern Radar*, vol.5, pp. 12-15, 2003.

[2] Zhu Mingbo, Zhao Zhenbo, Li Xiangping, "Trajectory optimization for missile-borne SAR imaging phase via gauss pseudospectral method," *IEEE CIE International Conference on Radar*, pp. 867-870., 2011.

[3] Yi Yusheng, Zhang Linrang, Liu Nan, Liu Xin, Shen Dong, "An efficient imaging algorithm for missile-borne side-looking SAR," *IET International Radar Conference*, pp. 1-4, 2009.

[4] Zhou Song, Bao Min, Zhou Peng, Xing Mengdao, Bao Zheng, "An imaging algorithm for missile-borne SAR with downward movement based on azimuth nonlinear chirp scaling," *Journal of Electronics & Information Technology*, vol. 33, No.6, pp. 1420-1426,2011.

[5] Zhang Donglei, Wang Feng, Li Yachao, "Improved chirp scaling algorithm for missile-borne SAR with high squint," *Journal of Astronautics*, vol. 32, No.6, pp. 1359-1364, 2011.

[6] Bao Zheng, Xing Mengdao, Wang Tong, *Radar Imaging Technolody*, Bejing: Publishing House of Electronics Industry, 2005, pp.146-151.
[7] Huaying Xie, Hongzhong Zhao, Qiang Fu, "Taylor expansion and its application in missile-borne SAR imaging," *APSAR*, pp. 426-430, 2009.
[8] Ian G.Cumming, Frank H.Wong, *Digital Processing of Synthetic Aperture Radar Data Algorithms and Implementation*, Norwood, MA: Artech House, 2005.
[9] Yew Lam Neo, Frank H.Wong, Iam G.Cumming, "Processing of azimuth-invariant bistatic SAR data using the range Doppler algorithm," *IEEE Trans on Geoscience and Remote Sensing*, vol.46, No.1, pp. 14-21, 2008.